

# Direct Observation of Langmuir Films of C<sub>60</sub> and C<sub>70</sub> Using Brewster Angle Microscopy

R. Castillo\* and S. Ramos

Instituto de Física, UNAM. P.O. Box 20-364, D.F. 01000, Mexico

J. Ruiz-Garcia

Instituto de Física, "Manuel Sandoval Vallarta", UASLP. Alvaro Obregon 64, San Luis Potosi, S.L.P. 78000, Mexico

Received: April 24, 1996; In Final Form: June 20, 1996<sup>⊗</sup>

The aim of this paper is to present a direct observation of Langmuir films made of C<sub>60</sub> and C<sub>70</sub> along the process of their compression at 298 K, using Brewster angle microscopy. We found coexisting a gas phase and a condensed phase at low area densities. Our results agree with the formation of multilayers even at low area densities (500–1000 Å<sup>2</sup>/molecule). We made compressions of the films at several speeds. Using dilute spreading solutions ( $\sim 1 \times 10^{-5}$  M) and slow compressions we obtained multilayers. With rapid compressions, we found that the condensed phase formed beautiful foamlike structures and circular domains of different sizes at very low area densities. The circular domains developed holes (gas bubbles). As the compression of the films proceeded, those domains did not coalesce easily. Instead, the films prefer to form multilayers. Using concentrated spreading solutions ( $> 1 \times 10^{-4}$  M) and slow compressions, multilayers were formed just after the deposition of the sample.

## Introduction

The discovery of the carbon fullerenes<sup>1</sup> has triggered a new field of research where a great variety of new carbon structures have been discovered. The development of a synthetic method to obtain macroscopic amounts of fullerenes<sup>2</sup> enhanced the interest in those molecules. That started a great variety of studies. In particular, thin films of fullerenes are of interest because they exhibit several interesting properties, among them we can mention superconductivity,<sup>3</sup> superconductivity upon reduction,<sup>4,5</sup> photo-electrochemical response,<sup>6</sup> and an interesting electrochemical behavior.<sup>7</sup> But, it is still controversial whether or not fullerenes, i.e., C<sub>60</sub> and C<sub>70</sub>, form a monolayer at the air–water interface. On the basis of the surface-pressure–area isotherms, some authors<sup>8–13</sup> have reported monolayer formation while others,<sup>3,14–20</sup> probably the most, have noted multilayer formation. For those in the later case, the limiting area per molecule calculated from the pressure–area isotherms yields a value too small, by a factor of almost 3, as compared with the value expected for the case of monolayer formation. This led them to conclude that fullerenes tend to aggregate at the air–water interface rather than forming a monomolecular layer. This conclusion is also supported by the lack of a hydrophilic moiety in fullerenes, as well as the readiness of fullerenes to form clusters in solution.<sup>21–23</sup> The controversy has continued, but no one has tried a direct observation of the films obtained in the experimental conditions reported by the different authors. Therefore, the aim of this paper is to present a direct observation of Langmuir films made of C<sub>60</sub> and C<sub>70</sub> along the process of compression at 298 K, using Brewster angle microscopy.<sup>24,25</sup>

The lack of liquid phase is another interesting property of C<sub>60</sub>. Although, C<sub>60</sub> is a nearly spherical molecule, its intermolecular potential is not of a Lennard-Jones type. A simple pair potential that should describe the intermolecular interactions of C<sub>60</sub> has been proposed,<sup>26</sup> where the ratio of the width of the attractive well to the diameter of the repulsive core of the potential is much less for C<sub>60</sub> than for the case of the Lennard-

Jones potential. The effect of this short range of the intermolecular interaction has been studied through Monte Carlo simulation.<sup>27</sup> The results have shown that the sublimation line passes above the liquid–vapor critical point ( $\sim 1798$  K), suggesting that C<sub>60</sub> has no stable liquid phase in three dimensions. This would be the first example of a pure substance that has no gas–liquid–solid triple point. If those simulations correspond to actual C<sub>60</sub>, direct observation of Langmuir monolayers made of C<sub>60</sub> never should show an expanded liquid phase, since the expanded liquid phase of a monolayer corresponds to the liquid in three dimensions, at least for the Lennard-Jones case.<sup>28</sup> As we will show below this is the case here. As far as we know, no one has studied phase transitions in C<sub>70</sub> through simulations.

The formation of highly incompressible and stable Langmuir monolayers of C<sub>60</sub> at the water–air interface was first reported by Obeng and Bard,<sup>8</sup> at temperatures in the range 5–35 °C. They found that the limiting area per molecule calculated from pressure–area ( $\pi$ -A) isotherms yielded a radius of 5.6 Å for the C<sub>60</sub> in the monolayer. They concluded that this limiting area was in good agreement with the data obtained from other techniques. Bulhoes, Obeng, and Bard<sup>9</sup> have given additional information about the proper experimental conditions to obtain Langmuir monolayers at the water–air interface such as C<sub>60</sub> concentration, sample size, trough conditions, etc. Although, as mentioned above, there are many authors who have failed to obtain them.<sup>3,14–20</sup>

Langmuir monolayers of C<sub>70</sub> at the water–air interface were first reported by Jehoulet et al.<sup>10</sup> at 25 °C. They deposited the films on a trough in the same manner as the C<sub>60</sub> films and reported two transitions in their  $\pi$ -A isotherms. The limiting areas for those transitions yielded radii of  $9.0 \pm 3.0$  and  $5.8 \pm 1.6$  Å, respectively. Then, they concluded that these values were in reasonable agreement with the theoretical values expected for the prolate spheroidal C<sub>70</sub> carbon cage in two configurations: namely one configuration corresponding to a monolayer film made up mainly of C<sub>70</sub> molecules with their long axes parallel to the interface at low pressure and another configuration

<sup>⊗</sup> Abstract published in *Advance ACS Abstracts*, August 1, 1996.

corresponding to the case in which the molecules predominantly stand up vertically at high pressure. For this case also other groups have failed to obtain monolayers.<sup>18</sup>

The C<sub>60</sub> molecules also formed stable mixed films at the air–water interface with some organic compounds with some amphiphilic character. Some examples can be found in the recent literature such as the cases of arachidic acid/C<sub>60</sub><sup>8,18,11</sup> and that of octadecanol/C<sub>60</sub>.<sup>29</sup> C<sub>70</sub> has also been used to form mixed films with arachidic acid. In a report, Jehoulet et al.<sup>10</sup> found that the  $\pi$ -A isotherm (25 °C) showed two transitions. The limiting radius in the fully compressed film was on the order of 7.8 Å, suggesting that, in contrast to the C<sub>60</sub>/arachidic acid films, the C<sub>70</sub> molecules in these films are much closer to the air–water interface and make a significant contribution to the ultimate final packing. The diameters for C<sub>70</sub> obtained by electron diffraction using a simulated annealing method<sup>30</sup> are 7.80 and 6.94 Å for the longest and the equatorial diameters, respectively, which are not much different from the 7.1 Å diameter of the C<sub>60</sub> molecule obtained from X-ray measurements.<sup>31</sup> Surprisingly, given the resemblance between molecules of C<sub>70</sub> and C<sub>60</sub>, the isotherms for the mixed films presented by those authors are quite different. In their work, the  $\pi$ -A isotherms for films made up of 1:1 C<sub>60</sub>/arachidic acid mixtures start to rise at ca. 28 Å<sup>2</sup>/molecule, while those films for 1:1 C<sub>70</sub>/arachidic acid mixtures start to rise at ca. 400 Å<sup>2</sup>/molecule. Recently, our group presented results for mixed Langmuir films made of C<sub>70</sub> and arachidic acid at several temperatures and concentrations.<sup>32</sup> Those results are different from those presented by Jehoulet et al.<sup>10</sup> and, as expected, closer to those of the C<sub>60</sub>/arachidic acid mixed films.

Quite recently, several works have been devoted to obtaining Langmuir films of fullerene derivatives. Some important examples can be mentioned, namely, films made of 1-*tert*-butyl-1,9-dihydrofullerene-60,<sup>15</sup> C<sub>60</sub>O and C<sub>61</sub>H<sub>2</sub>,<sup>12</sup> amphiphilic C<sub>60</sub> carboxylic acid,<sup>33</sup> of fullerene derivatives with a great variety of polar addends,<sup>34</sup> azacrown/fullerene complexes,<sup>35</sup> and of calixarene/fullerene complexes.<sup>36</sup>

## Experimental Section

**Reagents.** C<sub>60</sub> (>99.99% purity) and C<sub>70</sub> (>98% purity) were supplied by Mer Corp. (Tucson, AZ). Chloroform (HPLC grade, 99.9%) from Sigma–Aldrich (Sigma Chemical Co. and Aldrich Chemical Co., Inc.) was used for cleaning the trough. As subphase for all the Langmuir films, we used Millipore water (Super Q system, Millipore Corp. plus a 0.2 μm Barnsted filter at the end, model D3750, Barnsted/Thermolyne, IA) or Nanopure water (Nanopure-UV, model D7334, Barnsted/Thermolyne, IA). Dry benzene (chromatographic grade, >99.7%) was used as the solvent for the preparation of the fullerene spreading solution. This was supplied by Merck (Merck-Mexico, Mexico).

**Apparatus.** All films were prepared on a computerized Nima LB trough (MODEL TKB 2410A, Nima Technology LTD, England) using a Wilhelmy plate to measure the surface pressure. The trough was isolated from vibrations using a pneumatic tube incorporated into a steel base. The barriers are made of PTFE fitted with stiffening bars defining a working circular area, starting at 1000 cm<sup>2</sup>. All experiments were carried out in a dust-free environment.

The Brewster angle microscope (BAM) observations were performed in a BAM1 plus (Nanofilm Technologie GmbH, Germany) using the previous described trough and a 222 cm<sup>2</sup> Teflon rectangular Langmuir trough (R & K Ultrathin Organic Film Technology, Germany). The BAM analyzer gave the best contrast while kept at 0° or 180°.

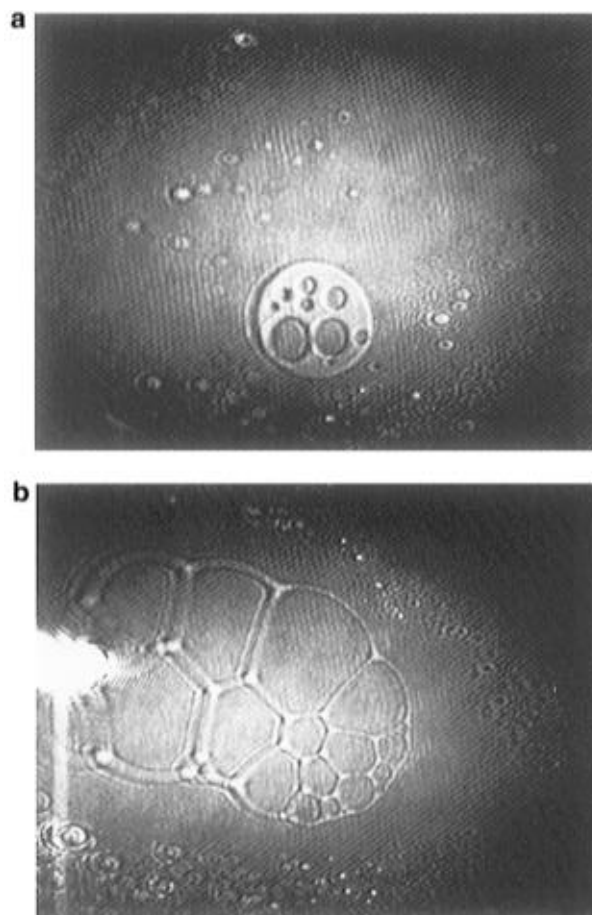


**Figure 1.** Films of C<sub>60</sub>. (a) Gas phase (dark areas) and circular domains of condensed phase (disks) with holes (gas phase bubbles). (b) Gas phase (dark areas) and foamlike structures of condensed phase. In all the figures the horizontal breadth corresponds to ca. 800 μm and the spatial resolution is ca. 4 μm.

The Nima LB trough and the BAM with its associated trough were placed on concrete tables cemented to a concrete floor on the ground floor of our building. The temperature in both troughs was kept constant with the aid of two water circulator baths (Cole-Parmer 1268-24 and Haake F3-K). The subphase was at constant temperature within a precision of 0.1 K.

**Procedure.** Fresh solutions of C<sub>60</sub> and of C<sub>70</sub> in benzene were deposited onto the unbuffered water subphase at the working temperature. Small amounts (5 μL) of these solutions were applied at several sites on the water surface with a 50 μL Hamilton syringe. After 5 min, this procedure was repeated until we had the desired quantity of the compound in the film. Then, after 20–30 min, the time allowed for solvent evaporation, the films were compressed in the Nima LB trough continuously, at 298 K.

## Results and Discussion

**Isotherms.** We measured the  $\pi$ -A isotherms for the C<sub>60</sub> and C<sub>70</sub> films for two cases, namely, one case using dilute spreading solution ( $\sim 1 \times 10^{-5}$  M) and another case using a concentrated spreading solution ( $> 1 \times 10^{-4}$  M). These cases correspond to those presented in Figure 2 of the work of Bulhoes et al.<sup>10</sup> In all our measurements we followed the suggestions given in that work and, consequently, we used benzene as solvent.

For the case when dilute spreading solutions were used, we started the compression of the films at a surface area in the range 29 000–10 000 Å<sup>2</sup>/molecule. Several compression rates

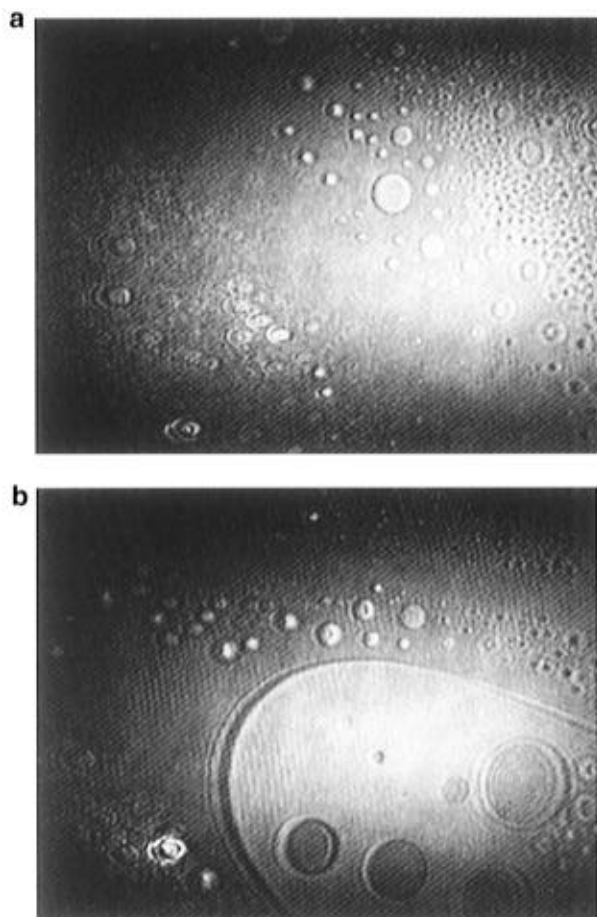


**Figure 2.** Films of C<sub>60</sub>. (a) Small circular disks of condensed phase. (b) Big disk of condensed phase, also with circular holes of gas phase inside, surrounded by small disks. Close to this big disk, there is a large spotted area of very small disks as those shown in part a.

(560–95 Å<sup>2</sup> molecule<sup>-1</sup> min<sup>-1</sup>) and sample sizes (50, 75, 100, and 150 μL) were used. We were unable to obtain an actual surface pressure measurement close to the claimed<sup>8–13</sup> surface area of film collapse (C<sub>60</sub>, ~96 Å<sup>2</sup>/molecule; C<sub>70</sub>, ~160 Å<sup>2</sup>/molecule). Due to the small quantities of fullerenes deposited onto the water surface, the available experimental area needed by the trough becomes very small (3–10 cm<sup>2</sup>). Here, the Teflon barriers modified the measured Π. They were so close that the height of the water surface in contact with the Wilhelmy plate changes substantially. Thus, we stopped the experiments approximately at 200–250 Å<sup>2</sup>/molecule. In a similar way, the small quantities of fullerenes did not allow us to use lower compression speeds due to limitations of our equipment (minimum speed 5 cm<sup>2</sup>/min). The surface pressure measurements were essentially constant (Π ~ 0 mN/m) from the beginning of the experiments until we stopped them. Here, authors claiming monolayer formation<sup>8–13</sup> assumed a gas-phase coexisting with a condensed phase monolayer. As we will mention below, BAM images do not support this assumption.

For the case of concentrated spreading solutions of C<sub>60</sub>, we started our compressions at a surface area in the range 850–450 Å<sup>2</sup>/molecule. The compression rate was in the range 21–10 Å<sup>2</sup> molecule<sup>-1</sup> min<sup>-1</sup> depending on the sample size (200–400 μL). We always obtained multilayer formation with limiting areas in the range 28–44 Å<sup>2</sup>/molecule. Our results are in close agreement with results for concentrated spreading solutions presented by Bulhoes, Obeng, and Bard<sup>9</sup> and with many researchers who failed to obtain monolayers.<sup>3,14–20</sup>



**Figure 3.** Films of C<sub>60</sub>. (a) Stripe of condensed phase with many holes with gas phase. In the center of the stripe there is a bright spot typically of a multilayer seed. Small disks and a spotted area are clearly shown outside the stripe. (b) Disk of condensed phase with holes of gas phase that has a bright spot probably due to a multilayer seed in the center. (c) Big hole with gas phase and small disks. Here, the brighter area is condensed phase surrounding gas phase. The condensed phase also has many small holes.

For the case of concentrated spreading solutions of C<sub>70</sub>, we started our compressions at a surface area in the range 550–250 Å<sup>2</sup>/molecule. The compression rate was around 16–8 Å<sup>2</sup> molecule<sup>-1</sup> min<sup>-1</sup> (sample size 500–1000 μL). We obtained isotherms very close to those isotherms for multilayers reported by Back and Lennox.<sup>18</sup> Our limiting areas were in the range of 32–50 Å<sup>2</sup>/molecule. Although, there were some isotherms for which the pressure started to increase steadily since 70–100 Å<sup>2</sup>/molecule. But, close to 40 Å<sup>2</sup>/molecule, the subphase

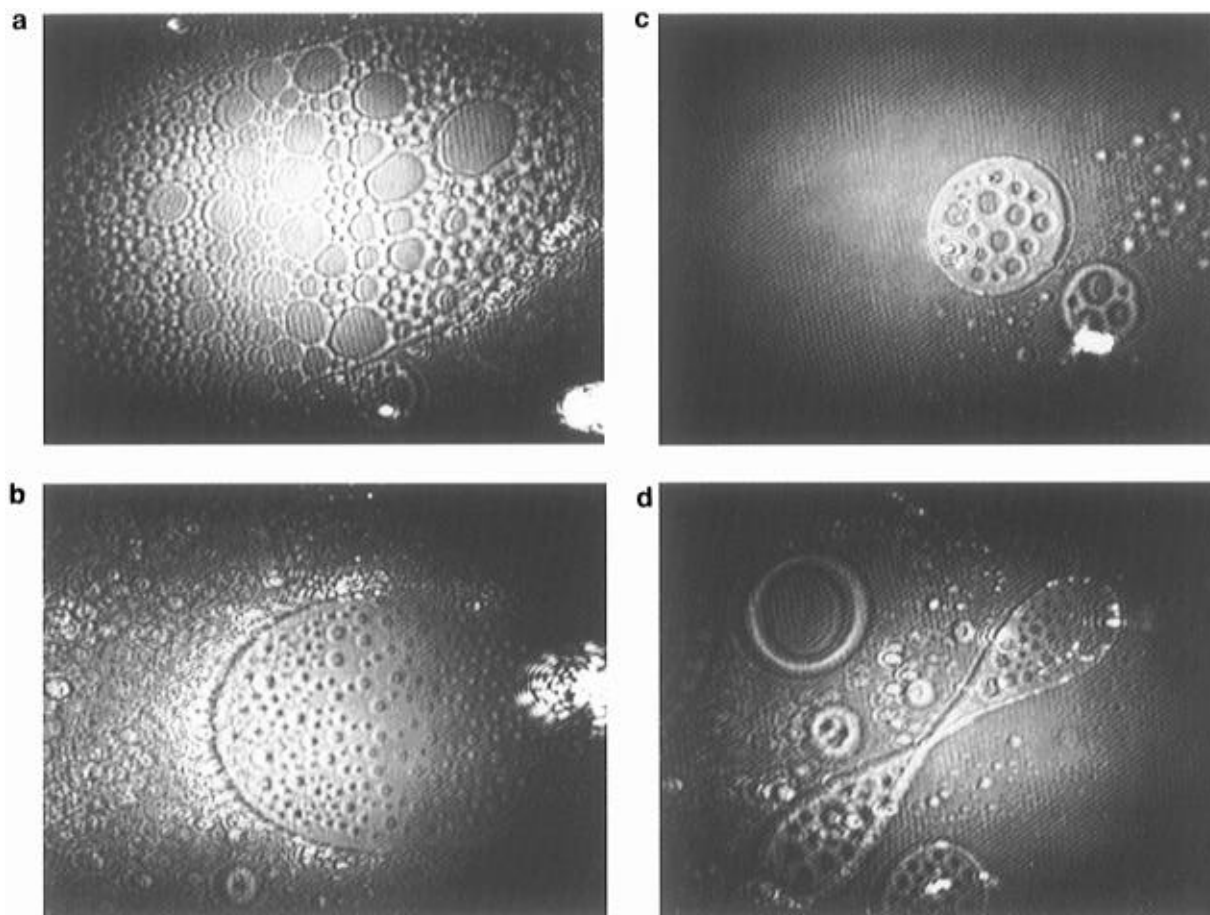


**Figure 4.** Films of  $C_{70}$ . (a) Foamlike structures of condensed phase. (b) Circular structures of condensed phase with gas phase holes. (c) Small disks and disks with holes. (d) Domains of condensed phase with holes with a “bow tie” shape.

surface showed a brown deposit over it. This clearly indicated the existence of multilayers.

**Brewster Angle Images.**  $C_{60}$  and  $C_{70}$  were deposited onto the water–air interface. The films were observed with Brewster angle microscopy, during the process of their compression at 298 K. We present here two cases, depending on the concentration of the spreading solutions:

(a) *Dilute Spreading Solution* ( $\sim 1 \times 10^{-5} M$ ). The procedure in both cases, for  $C_{60}$  and for  $C_{70}$ , was the following: Prior deposition onto the water–air surface, we observed the surface to verify that there were no surface-active contaminants on it. Then, 25  $\mu\text{L}$  of dilute solution were deposited on the water surface, and after some waiting time to allow solvent evaporation ( $\sim 0.5$  h), some observations with the BAM were made to verify that there were no multilayers. Afterward, we added another 25  $\mu\text{L}$  of dilute solution and repeated the cycle. Then, after further waiting ( $\sim 0.5$  h) the compression started.

As we noted that the speed of compression could be an important parameter to take into account, we made several experiments at the lowest speed of compression allowed in our experiment, 95  $\text{\AA}^2 \text{ molecule}^{-1} \text{ min}^{-1}$ . This lowest speed of compression value is actually not as low as commonly used, but it is determined by the very small concentration of fullerenes onto the surface and the lowest compression speed of our trough (minimum speed 5  $\text{cm}^2/\text{min}$ ). Also, we made experiments in a quasi-static way, i.e., compressing 20  $\text{cm}^2$  and waiting 2 min. At the beginning of compression, we observed as expected, very wide areas of gas phase (dark areas) coexisting with small irregular grains. The images of the grains were very bright, and we were unable to focus them. As the compression proceeds the grains increased in number and size. This events

occurred at very early stages in the compression process (13 600–2000  $\text{\AA}^2/\text{molecule}$ ). This evidence made clear to us that fullerenes deposited onto the air–water surface tend to form multilayers.

Unexpectedly, as we increased the speed of compression, we observed the formation of a very different kind of condensed phase structures. Below, we will describe our BAM observations of several experiments for which the speed of compression was in the range 560–180  $\text{\AA}^2 \text{ molecule}^{-1} \text{ min}^{-1}$  ( $\sim 20 \text{ cm}^2/\text{min}$ ):

For the case of the  $C_{60}$ , compressions of the films started at a very large area per molecule ( $\sim 29\,000 \text{ \AA}^2/\text{molecule}$ ) with a nondetectable surface pressure. Here, we found coexisting a gas phase and a condensed phase. The condensed phase can be focused easily, and apparently, it has a uniform thickness. At the beginning of compression, we observed very wide areas of gas phase (dark areas) and some condensed phase structures forming circular domains (disks) of different sizes and foamlike structures as shown in Figures 1a,b (the denser the phase the brighter the BAM). In all the figures the horizontal breadth corresponds to ca. 800  $\mu\text{m}$  and the spatial resolution is ca. 4  $\mu\text{m}$ . The larger circular domains usually showed holes inside (gas phase bubbles), while small domains looked like perfect circular disks. The area where our BAM is in focus is not very large. Thus, some parts of the images shown are not completely in focus. This situation is quite different when one is wandering over the liquid surface with the microscope, since oneself can move freely at will to observe in focus every section of a whole structure. Those mentioned structures were surrounded by many very small disks that are difficult to focus in the whole view, because of their size. However, they can be observed clearly

when they are specifically focused. When many of them are presented in an image, it appears to be spotted, like a superposition of many Newton rings. Those small circular disks can be easily seen in Figures 2a,b. In particular, in Figure 2b, we can see there a very big disk also with circular holes of gas phase inside, surrounded by small disks. Also close to this big disk, there is a large spotted area of those very small disks. We believe that those very small disks probably have some holes, but due to the BAM resolution, it is not possible to observe them. After some time of observation and continuous compression, larger disks of all sizes were observed, all of them having holes with gas phase. Foamlike structures were observed only occasionally, and usually, they were quite stable. They did not change much during the observation time. It is not clear what kind of mechanism triggers the formation of those structures. The formation of foam structures by condensed phases is quite unusual. As far as we know, there is only one report of a foam formation by a liquid condensed phase in coexistence with a liquid expanded phase.<sup>37</sup> Therefore, this is the first report of foam formation by a condensed phase in coexistence with a gas phase.

Figures 3a–c are examples of some of the structures found during the compression process (29 000–2000 Å<sup>2</sup>/molecule). In Figure 3a, there is a stripe with many holes with gas phase. Here, in the center of the stripe, there is a bright spot of the type of multilayers. It looks like a multilayer seed. Most of the observed structures have the same kind of seed (they look as those grains mentioned in the quasi-static or very slow speed of compression experiments). In Figure 3b, we can see a beautiful disk with holes of gas phase that has a bright spot probably due to a multilayer seed in the center. Figure 3c presents a big hole with gas phase and small disks. Here, the brighter area is condensed phase surrounding gas phase. The condensed phase also has many small holes. In all the observations, we used the beam analyzer to find some evidence of regions of different molecular orientation in the condensed phase. As expected, that was not the case.

As far as the compression continues, the number of small disks increased and, as a consequence, the size of spotted areas formed by the small disks also increased, see Figure 3a. Close to 80–120 Å<sup>2</sup>/molecule, we never observed a monolayer. We always observed spotted areas formed with very small disks now impossible to focus, probably because they have different heights. Although, there were some surviving structures of those mentioned above, most of the views were spotted areas. The increase in reflectivity and the difficulty of focusing those very small disks convinced us that we were observing small disks with several layers (similar to what is observed outside the stripe of Figure 3a). At a lower area per molecule (<100 Å<sup>2</sup>/molecule), the surface appeared as a bright spotted area, clearly not a monolayer. All our observations are consistent with a picture of very small disks that are not prone to coalesce. Therefore, as they are forced by compression to coalesce, they prefer to form multilayers instead of healing and of coalescing. This probably only shows the tendency of C<sub>60</sub> to avoid the water surface, because of its lack of a hydrophilic moiety.

The rapid compressions of the C<sub>70</sub> were carried out in the same way as for C<sub>60</sub>. The compression started at very large area per molecule (~30 000 Å<sup>2</sup>/molecule) and with a nondetectable surface pressure. Here, we also found coexisting a gas phase and a condensed phase. At the beginning of the compression, as in the case of C<sub>60</sub>, we observed very wide areas of gas phase (dark areas) and only some structures of condensed phase. The condensed phase formed the same kind of structures as in the case of C<sub>60</sub>, i.e., foamlike structures (Figure 4a), circular

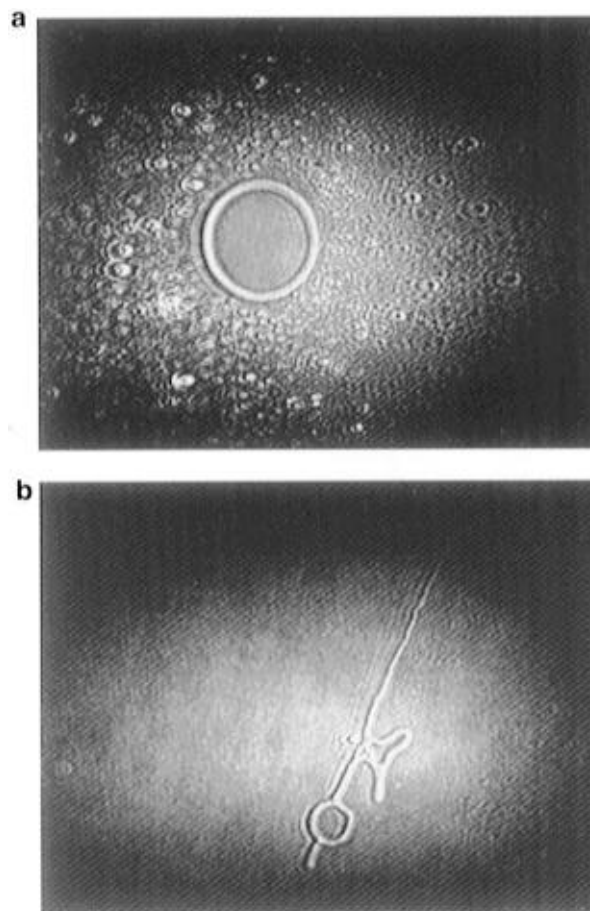


**Figure 5.** Films of C<sub>70</sub>. (a) Ring-shaped structure of condensed phase. (b) Thread-shaped structure of condensed phase.

structures with holes of gas phase (Figures 4b,c), and small disks (Figure 4c). Also, we found in this case circular domains with holes with a “bow tie” shape (Figure 4d). We noted that the C<sub>70</sub> condensed phase structures have, qualitatively, more holes than those condensed phase structures of C<sub>60</sub>. Besides, C<sub>70</sub> shows other kinds of structures not shown by C<sub>60</sub>, such as ring-shaped structures (Figure 5a) and thread-shaped structures (Figure 5b). However, those structures were not abundant throughout the surface. All the mentioned structures are surrounded by many small disks, as in the case of C<sub>60</sub>, and are also difficult to focus in the whole view because they are very small, too. In addition, as they increase in number the image becomes spotted. Figures 4b,d and 5a present spotted areas that correspond to disks out of focus. In C<sub>70</sub>, multilayers are more clear than in C<sub>60</sub> (see Figure 6). Close to an area of 1000 Å<sup>2</sup>/molecule, we could observe very clearly condensed phase layers (terraces), one partially above another. We clearly observed holes in the upper layer, disks over the lower layer, and the step. Also associated to those multilayers, we found high reflectivity multilayer seeds and spotted areas made up of small disks. As the compression reaches values close to 160 Å<sup>2</sup>/molecule, where the pressure is supposed to increase,<sup>10</sup> we observed only high reflectivity spotted areas (multilayers) impossible to focus.

(b) *Concentrated Spreading Solution (>1 × 10<sup>-4</sup> M).* With concentrated spreading solutions, the situation was very different since multilayers appeared quite early (>1000 Å<sup>2</sup>/molecule) as very large domains. In some cases, it is very easy to observe the difference in height of the layers, as shown in Figure 7 for C<sub>60</sub> (at 90 Å<sup>2</sup>/molecule) and in Figure 8 for C<sub>70</sub> (468 Å<sup>2</sup>/molecule). In Figure 9, we observe large areas (solid domains)

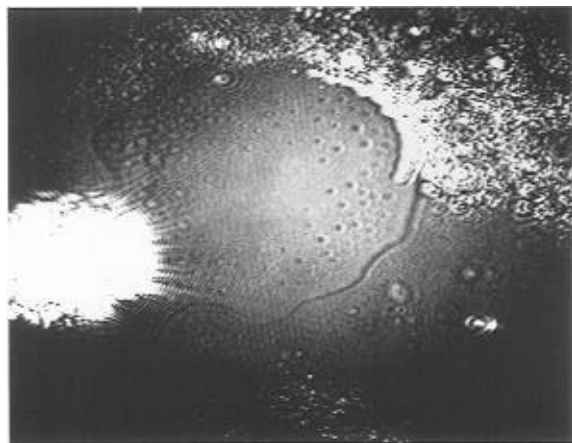


**Figure 6.** Condensed phase terraces of  $C_{70}$ . This figure shows an upper layer with holes, disks over the lower layer, and the step. Also associated to those multilayers, there are high reflectivity multilayer seeds and spotted areas made up of small disks ( $1000 \text{ \AA}^2/\text{molecule}$ ).



**Figure 7.** Multilayers of  $C_{60}$  at  $90 \text{ \AA}^2/\text{molecule}$  formed with a concentrated spreading solution.

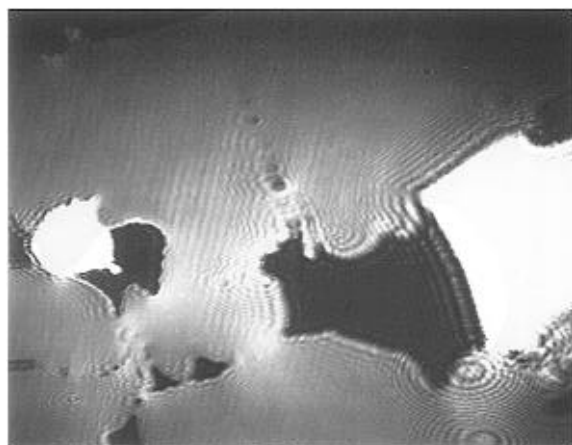


**Figure 8.** Multilayers of  $C_{70}$  at  $468 \text{ \AA}^2/\text{molecule}$  formed with a concentrated spreading solution.

with different reflected intensities, as well as very dark areas of gas phase. In all cases, the analyzer was rotated to ensure that the difference in intensity does not correspond to molecular orientation.  $C_{70}$  shows exactly the same pattern as can easily be seen in Figure 8. Most of the structures shown are quite rigid, and during compression, it was easy to see how breakable they are. Those multilayer films in both cases,  $C_{60}$  and  $C_{70}$ , do not coalesce easily. Therefore, at the end of the compression the films clearly have not uniform height.

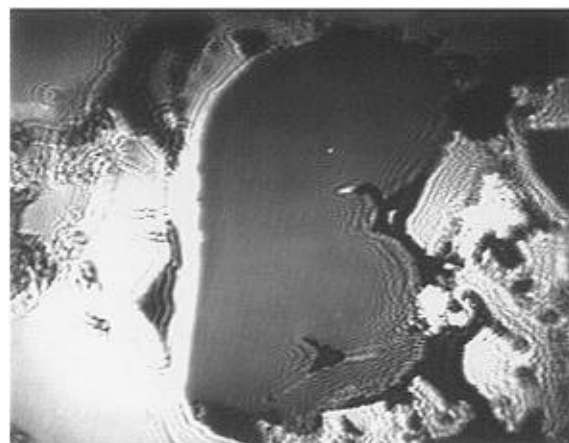


**Figure 9.** Multilayers of  $C_{60}$ . Solid domains with different reflected intensities, as well as very dark areas of gas phase.

In summary, we have shown by direct observation that fullerenes do not form stable monolayers on the water–air surface along the process of compression at 298 K, using Brewster angle microscopy. In particular, we were not able to reach the monolayer limiting areas claimed<sup>8–13</sup> ( $C_{60}$ ,  $\sim 96 \text{ \AA}^2/\text{molecule}$ ;  $C_{70}$ ,  $\sim 160 \text{ \AA}^2/\text{molecule}$ ), but we observed multilayer formation before reaching those areas. In addition, we found that the condensed phases formed several structures when the film undergoes compression at relatively large speeds. However, it is necessary to understand the way and the mechanisms under which those structures are formed. This work is underway.

**Acknowledgment.** We acknowledge the partial support of DGAPAUNAM Project IN100595 and of CONACYT Grants 0134PE9506 and 2027E9302.

## References and Notes

- (1) Kroto, H. W.; Heath, L. R.; O'Brian, S. C.; Curl, R. F.; Smalley, R. E. *Nature* **1985**, *318*, 162.
- (2) Kraetschmer, W.; Lamb, I. D.; Fostiropoulos, K.; Huffman, D. R. *Nature* **1990**, *347*, 354.
- (3) Wang, P.; Metzger, R. M.; Bandow, S.; Maruyama, Y. *J. Phys. Chem.* **1993**, *97*, 2926.
- (4) Murphy, D. W.; Rosseinsky, M. J.; Haddon, R. C.; Ramirez, A. P.; Hebard, A. F.; Tycho, R.; Fleming, R. M.; Dabbagh, G. *Physica C* **1991**, *185*, 403.
- (5) Allemand, P. M.; Khemani, K. C.; Koch, A.; Wudl, F.; Holczer, K.; Donovan, S.; Grüner, G.; Thompson, J. D. *Science* **1991**, *253*, 301.
- (6) Jehoulet, C.; Bard, A. J.; Wudl, F. *J. Am. Chem. Soc.* **1991**, *113*, 5457.
- (7) Dubois, D.; Kadish, K. N.; Flanagan, S.; Haufler, R. E.; Wilson, L. J. *J. Am. Chem. Soc.* **1991**, *113*, 7773.
- (8) Obeng, Y. S.; Bard, A. J. *J. Am. Chem. Soc.* **1991**, *113*, 6279.
- (9) Bulhoes, L. O.; Obeng, Y. S.; Bard, A. J. *Chem. Matter.* **1993**, *5*, 110.
- (10) Jehoulet, C.; Obeng, Y. S.; Kim, Y. T.; Zhou, F.; Bard, A. J. *J. Am. Chem. Soc.* **1992**, *114*, 4237.
- (11) Xiao, Y.; Yao, Z.; Jin, D.; Yan, F.; Xue, Q. *J. Phys. Chem.* **1993**, *97*, 7072.
- (12) Maliszewskyj, M. C.; Heiney, P. A.; Jones, D. R.; Strigin, R. M.; Cichy, M. A.; Smith, A. B. *Langmuir* **1993**, *9*, 1439.
- (13) Xiao, Y.; Yao, Z.; Jin, S. *J. Phys. Chem.* **1994**, *98*, 5557.
- (14) Nakamura, T.; Tachibana, H.; Yumura, M.; Matsumoto, M.; Azumi, R.; Tanaka, M.; Kawabata, Y. *Langmuir* **1992**, *8*, 4.
- (15) Goldenberg, L. M.; Williams, G.; Bryce, M. R.; Monkman, A.P.; Petty, M. C.; Hirsch, A.; Soi, A. *J. Chem. Soc., Chem. Commun.* **1993**, 1310.
- (16) William, G.; Pearson, C.; Bryce, M. R.; Petty, M. C. *Thin Solid Films* **1992**, *209*, 150.
- (17) Wang, Y. M.; Kamat, P. V.; Patterson, L. K. *J. Phys. Chem.* **1993**, *97*, 8793.
- (18) Back, R.; Lennox. *J. Phys. Chem.* **1992**, *96*, 8149.

- (19) Wang, P.; Shamsuzzoha, M.; Wu, X. L.; Lee, W. J.; Metzger, R. M. *J. Phys. Chem.* **1992**, *96*, 9025.
- (20) Guo, J.; Xu, Y.; Li, Y.; Yang, C.; Yao, Y.; Zhu, D.; Bai, C. *Chem. Phys. Lett.* **1992**, *195*, 625.
- (21) Bezmelnitsin, V. N.; Eletsii, A. V.; Stepanov, E. V. *J. Phys. Chem.* **1994**, *98*, 6665.
- (22) Honeychuck, R. V.; Cruger, T. W.; Milliken, J. A. *J. Am. Chem. Soc.* **1993**, *115*, 3034.
- (23) Sun, Y. P.; Bunker, C. E. *Nature* **1993**, *365*, 398.
- (24) Hénon, S.; Meunier. *Rev. Sci. Instrum.* **1991**, *62*, 936.
- (25) Hönig, D.; Möbius. *J. Phys. Chem.* **1991**, *95*, 4590.
- (26) Girifalco, L. A. *J. Phys. Chem.* **1992**, *96*, 858.
- (27) Hagen, M. H.; Meijer, E. J.; Mooij, G. C. A.; Frenkel, D.; Lekkerkerker, H. N. W. *Nature* **1993**, *365*, 425.
- (28) Abraham, F. F. *Physics Rep.* **1981**, *80*, 339.
- (29) Milliken, J.; Dominguez, D.; Nelson, H. H.; Barger, W. R. *Chem. Matter.* **1992**, *4*, 252.
- (30) McKenzie, D. R.; Davis, C. A.; Cockayne, D. J. H.; Muller, D. A.; Vassallo, A. M. *Nature* **1992**, *355*, 622.
- (31) Heiney, P. A.; Fisher, J. E.; McGhie, A. R.; Romanow W. J.; Denesten, A. M.; McCauley, J. P.; Smith, A. B. *Phys. Rev. Lett.* **1991**, *66*, 2911.
- (32) Castillo, R.; Ramos, S.; Ruiz-Garcia, J.; Varea, C. *Fluid Phase Equilib.* **1995**, *110*, 129.
- (33) Matsumoto, M.; Tachibana, H.; Azumi, R.; Tanaka, M.; Nakamura, T. *Langmuir* **1995**, *11*, 660.
- (34) Jonas, U.; Cardullo, F.; Belik, P.; Diederich, F.; Gügel, A.; Harth, E.; Herrmann, A.; Isaacs, L.; Müllen, Ringsdorf, H.; Thilgen, C.; Uhlmann, P.; Vasella, A.; Waldruff, C. A. A.; Walter, M. *Chem. Eur. J.* **1995**, *1*, 243.
- (35) Diederich, F.; Effing, J.; Jonas, U.; Jullien, L.; Plesniviy, T.; Ringsdorf, H.; Thilgen, C.; Weinstein, D. *Angew. Chem., Int. Ed. Engl.* **1992**, *31*, 1599.
- (36) Castillo, R.; Ramos, S.; Cruz, R.; Martinez, M.; Lara, F.; Ruiz-Garcia, J. *J. Phys. Chem.* **1996**, *100*, 709.
- (37) Stine, K. J.; Bono, M. F.; Kretzer, J. S. *J. Colloid Interface Sci.* **1994**, *162*, 320.

JP961186K